IEEE Access
Multidisciplinary ⋮ Rapid Review ⋮ Open Access Journal

Received November 1, 2020, accepted November 24, 2020, date of publication November 30, 2020,
date of current version December 17, 2020.

*Digital Object Identifier 10.1109/ACCESS.2020.3041418*

# Compact Mode Division MUX/DEMUX Using Enhanced Evanescent-Wave Coupling on Silicon-on-Insulator (SOI) Platform for 11-Tbit/s Broadband Transmission

**GUAN-HONG CHEN[1], JUI-FENG TSAI[1], CHING-WEI PENG[1], PIN-CHENG KUO[1], CHUN-JUI CHEN[1], CHI-WAI CHOW[1], (Senior Member, IEEE), CHIEN-HUNG YEH[2], (Member, IEEE), YINCHIEH LAI[1], (Member, IEEE), AND YANG LIU[3]**

[1]Department of Photonics, College of Electrical and Computer Engineering, National Chiao Tung University, Hsinchu 30010, Taiwan
[2]Department of Photonics, Feng Chia University, Taichung 40724, Taiwan
[3]Philips Electronics Hong Kong Ltd., Hong Kong

Corresponding authors: Chi-Wai Chow (cwchow@faculty.nctu.edu.tw) and Chien-Hung Yeh (yehch@fcu.edu.tw)

This work was supported by the Ministry of Science and Technology, Taiwan, under Grant MOST-109-2221-E-009-155-MY3, Grant MOST-109-2224-E-009-002, and Grant MOST-107-2221-E-009-118-MY3.

**ABSTRACT** Mode-division-multiplexing (MDM) can increase the total on-chip transmission capacity. Silicon-on-insulator (SOI) based MDM multiplexer (MUX) and demultiplexer (DEMUX) using asymmetrical directional couplers (ADCs) are promising; however, they usually require long coupling lengths for mode conversion. Here, for the first time up to the authors' knowledge, we propose, simulate, fabricate and demonstrate a size reduced SOI based 4 × 4 MDM MUX and DEMUX using enhanced evanescent-wave coupling (EEC). Here, we illustrate by experiments and numerically analyses that by size reducing the ADC access coupling region, evanescent-wave coupling is enhanced. Significant coupling length reduction of ∼80 % can be achieved, while similar MDM MUX and DEMUX performance can be observed. To experimentally evaluate the broadband and high-speed transmission operations of the proposed device, 48 wavelength channels each modulated by >60 Gbit/s orthogonal frequency division multiplexing (OFDM) signals are successfully mode multiplexed and demultiplexed, achieving a transmission capacity of 11.73 Tbit/s.

**INDEX TERMS** Silicon photonics (SiPh), mode division multiplexing (MDM), orthogonal-frequency-division-multiplexing (OFDM).

## I. INTRODUCTION

The bandwidth demands are increasing very rapidly due to the popularity of video-based and cloud-based services. Inside the data center networks, the speeds of electronic interconnects are limited by the high heat density. Using silicon photonics (SiPh) technology can offer an increase in interconnect throughput with reduced power consumption [1]–[5]. By using the mature complementary metal oxide semiconductor (CMOS) fabrication technique, high performance and yield SiPh devices were fabricated [6]–[13]. To improve the transmission capacity of the SiPh interconnects, different multiplexing techniques have been proposed, such as wavelength division multiplexing (WDM), spatial division multiplexing (SDM) or polarization division multiplexing (PolDM). Among them, SDM allows signals to be transmitted in different cores [14] or different orthogonal eigenmodes in a core. The latter is also known as mode division multiplexing (MDM). Implementation of MDM systems using few-mode optical fiber (FMF) were reported. Some all-fiber MDM multiplexers (MUXs) and demultiplexers (DEMUXs) were proposed and fabricated, such as all-fiber directional mode selective couplers (MSCs) [15], [16], long period fiber grating (LPFG) [17], [18] and photonic lanterns (PLs) [19], [20]. Mode MUX/DEMUX using free-space optical setups were also reported [21].

On the contrary, deploying MDM in SiPh chip is relatively simpler, since distinct eigenmodes could be converted

The associate editor coordinating the review of this manuscript and approving it for publication was Leo Spiekman.

easily by the planar waveguide structures. The MDM MUX/DEMUX based on multimode interferences (MMIs) were proposed; however, the scalability may be limited [22], [23]. MDM MUX using quasi-phase-matching and staged coupling method was also reported; however, the size was relatively large [24]. High performance MDM MUX and DEMUX based on asymmetrical directional couplers (ADCs) were proposed [25], [26]. Through phase-matching the access and bus waveguides, fundamental mode and higher order modes can be converted efficiently. By using this ADC-based MDM MUX and DEMUX, several high throughput demonstrations were reported [27]–[29]. Yet, these MDM MUX and DEMUX required relatively long coupling lengths in the directional coupler section for mode conversion.

In this work, for the first time up to the authors' knowledge, we propose, simulate, fabricate and demonstrate a size reduced semiconductor-on-insulator (SOI) based 4 × 4 mode MUX/DEMUX using enhanced evanescent-wave coupling (EEC). Traditional SOI based mode MUX/DEMUX required relatively long coupling lengths in the directional coupler section for mode conversion. In this work, we illustrate that via reducing the dimension of the ADC access coupling region, evanescent-wave coupling is enhanced. A significant coupling length reduction of ∼80 % can be achieved, while similar mode MUX/DEMUX performance can be observed. Moreover, in order to evaluate the broadband and high-speed operations of the proposed footprint reduced EEC MDM MUX and DEMUX, 48 wavelength channels, each encoded with > 60 Gbit/s orthogonal frequency division multiplexing (OFDM) signals are mode multiplexed and demultiplexed successfully by using the proposed 4 × 4 mode MUX and DEMUX. The 48 C-band wavelength channels from 1527.99 nm to 1565.50 nm under the International Telecommunication Union (ITU) dense wavelength division multiplexing (DWDM) grid are selected. Hence, transmission capacity of 11.73 Tbit/s is achieved, and the hard-decision forward-error-correction (HD-FEC) threshold (bit-error-ratio, BER 3.8 × $10^{-3}$) is satisfied.

## II. DEVICE STRUCTURES AND NUMERICAL ANALYSIS

Fig. 1(a) illustrates the schematic of the proposed SiPh 4 × 4 MDM MUX/DEMUX. An ADC consists of a narrow access waveguide (supporting fundamental transverse-electric, $TE_0$ mode) and a wide bus waveguide (supporting high order modes). Within the coupling region, fundamental $TE_0$ mode can be converted to higher order modes (i.e. $TE_1$, $TE_2$, $TE_3$) or vice versa depending on specific widths of bus waveguides satisfying the phase-matching conditions [25]. Traditionally, the smallest SOI waveguide dimension for fundamental mode transmission is 0.45 $\mu$m × 0.22 $\mu$m. By reducing the width of the ADC access width, evanescent coupling can be enhanced and the coupling length (*LC*) can be significantly reduced.

Both proposed and traditional MDM MUX and DEMUX were fabricated by IMEC. They were put side-by-side on the same SOI wafer for comparison. Fig. 1(b) depicts the microscopic image of the proposed device with silicon waveguide

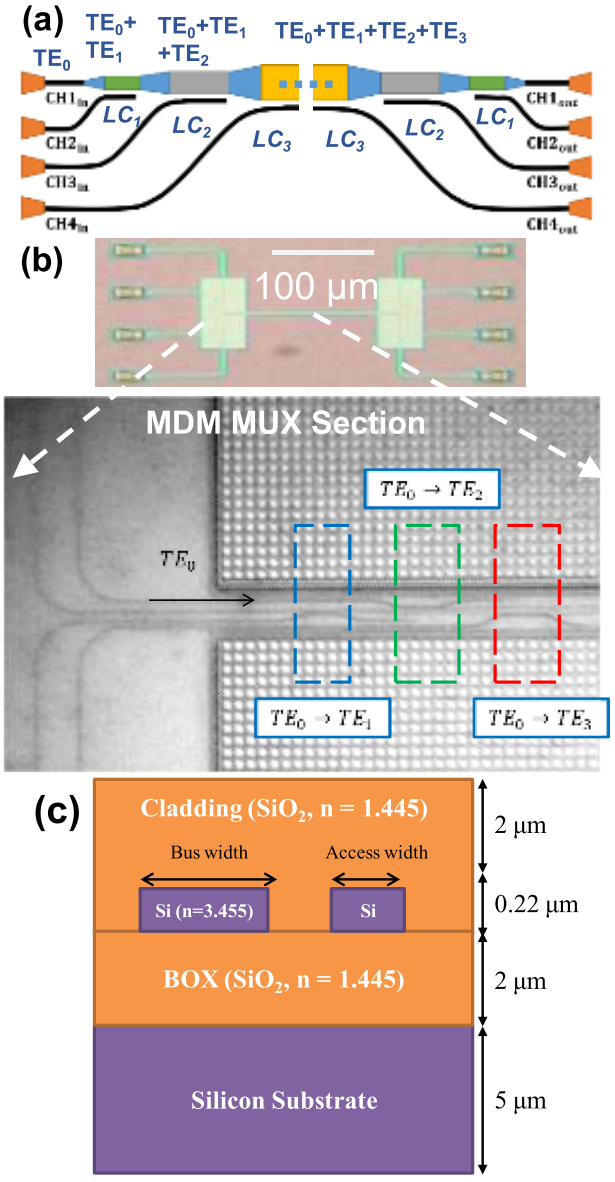


**FIGURE 1.** (a) Proposed 4 × 4 MDM MUX/DEMUX using EEC coupling. LC: coupling length. TE: transverse-electric. (b) Photo of the whole proposed device and a magnified MDM MUX section. (c) The cross section of the bus and access waveguides at the ADC section showing different material types.

thickness of 220 nm and the ADC gap of 150 nm. Fig. 1(b) is a magnified photo showing the access and bus waveguides, and the mode MUX regions of $TE_0$-to-$TE_1$, $TE_0$-to-$TE_2$, $TE_0$-to-$TE_3$. The optical signal at $TE_0$ mode can be coupled into and out of the MDM MUX and DEMUX via 10° off-vertical grating coupler (GC). The bus waveguide widths supporting different higher order modes can be calculated based on the phase-matching conditions [25], [27]. Lumerical® finite-difference time-domain (FDTD) method was used to simulate the devices. For the traditional MDM MUX/DEMUX, the access waveguide width supporting $TE_0$ mode is 0.45 $\mu$m; while the bus waveguide widths supporting the $TE_1$, $TE_2$ and

$TE_3$ are 0.932 $\mu$m, 1.416 $\mu$m and 1.897 $\mu$m respectiv2ely. The corresponding coupling lengths are 17 $\mu$m, 22.5 $\mu$m and 26.4 $\mu$m respectively. For the proposed reduced footprint MDM MUX/DEMUX, the access waveguide width supporting $TE_0$ mode is 0.35 $\mu$m. The bus waveguide widths supporting the $TE_1$, $TE_2$ and $TE_3$ are 0.740 $\mu$m, 1.132 $\mu$m and 1.535 $\mu$m respectively while the corresponding coupling lengths are reduced to 3.03 $\mu$m, 4.32 $\mu$m and 6.17 $\mu$m respectively. The cross section of the bus and access waveguides at the ADC section showing different material types is illustrated in Fig. 1(c).

Table 1 summaries the coupling lengths and bus waveguide widths of the two MDM devices. In the proposed size reduced EEC MDM device, the coupling lengths are significantly reduced by 82.2 %, 80.8 % and 76.6 % in CH2, CH3 and CH4 respectively; while the bus waveguide widths are reduced by 20.6 %, 20.1% and 19.1%, respectively.

**TABLE 1. Comparison of traditional MDM and proposed MDM.**

| | **Traditional CH2** | **Proposed CH2** |
|---|---|---|
| Coupling Length (μm) | 17.0 | 3.03 (↓82.2 %) |
| Bus Waveguide Width (μm) | 0.932 | 0.740 (↓20.6 %) |
| | **Traditional CH3** | **Proposed CH3** |
| Coupling Length (μm) | 22.5 | 4.32 (↓80.8 %) |
| Bus Waveguide Width (μm) | 1.416 | 1.132 (↓20.1 %) |
| | **Traditional CH4** | **Proposed CH4** |
| Coupling Length (μm) | 26.4 | 6.17 (↓76.6 %) |
| Bus Waveguide Width (μm) | 1.897 | 1.535 (↓19.1 %) |

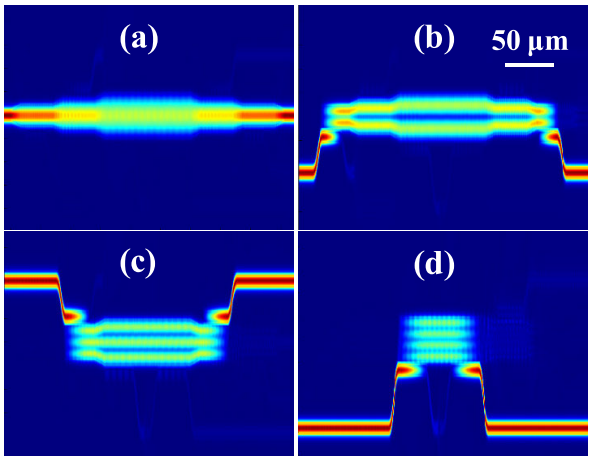


**FIGURE 2.** FDTD simulation of (a) $TE_0$, (b) $TE_0$ to $TE_1$ and vice versa, (c) $TE_0$ to $TE_2$ and vice versa, (d) $TE_0$ to $TE_3$ and vice versa in the traditional MDM device (access waveguide width of 0.45 $\mu$m).

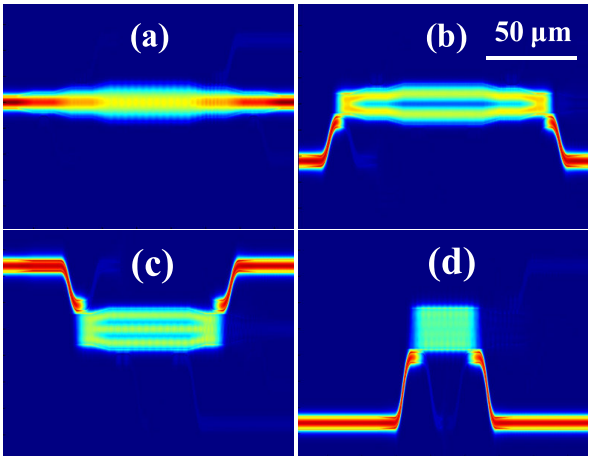


**FIGURE 3.** FDTD simulation of (a) $TE_0$, (b) $TE_0$ to $TE_1$ and vice versa, (c) $TE_0$ to $TE_2$ and vice versa, (d) $TE_0$ to $TE_3$ and vice versa in the traditional MDM device (access waveguide width of 0.35 $\mu$m).

Fig. 2 and Fig. 3 display the results of FDTD simulation by Lumerical®when light is propagating along the traditional and proposed MDM MUX and DEMUX. Figs. 2(a) and 3(a) show the fundamental $TE_0$ mode launching from the left hand side can maintain the same $TE_0$ mode at the output. Figs. 2(b)-(d) and 3(b)-(d) show that the fundamental $TE_0$ mode can be successfully converted to $TE_1$, $TE_2$, $TE_3$ or vice versa respectively by the traditional and the proposed MDM MUX and DEMUX. Simulation results show that in both traditional and proposed MDM devices, the optical power coupling efficiencies can achieve $> 95$ %.

Figs. 4(a)-(d) and 5(a)-(d) show the simulated normalized mode crosstalk observed at different output ports when the fundamental $TE_0$ mode optical signal is launched at the MDM channel 1 (CH1) to channel 4 (CH4) in both traditional and proposed MDM MUX/DEMUX devices respectively. The highest mode crosstalk can be observed in CH2 input at wavelength of 1525 nm as shown in Figs. 4(b) and 5(b). In general, both the traditional and proposed MDM devices reveal similar performances in the mode crosstalk analysis. The mode crosstalk is $<-20$ dB within the 40 nm C-band wavelength window from 1525 nm to 1565 nm.

## III. EXPERIMENTAL RESULTS AND DISCUSSION

The experimental evaluations of the traditional and proposed footprint reduced MDM MUX and DEMUX are performed. To evaluate the MDM mode crosstalk, a broadband light source using the amplified spontaneous emission (ASE) of an erbium-doped fiber amplifier (EDFA) is launched into each MUX input. Then different DEMUX outputs are measured by using an optical spectrum analyzer (OSA). For example, to measure the mode crosstalk of CH1 as shown in Fig. 6(a), the broadband light source is launched into the input port of MDM-CH1; and the optical spectra at the four output ports of MDM-CH1, MDM-CH2, MDM-CH3 and MDM-CH4 are measured. Then, the optical spectra measured at the four output ports are power normalized with respect to

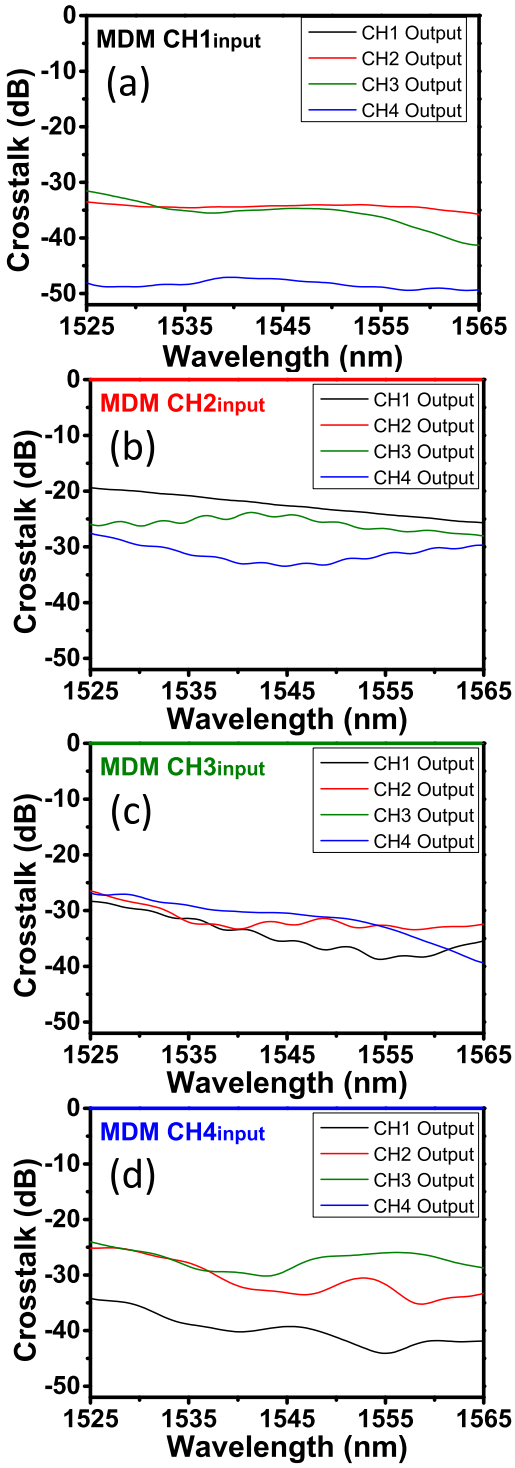


**FIGURE 4.** Simulated mode crosstalk at output ports while the input optical signal is launched at (a) CH1, (b) CH2, (c) CH3 and (d) CH4 in the traditional MDM MUX/DEMUX device.

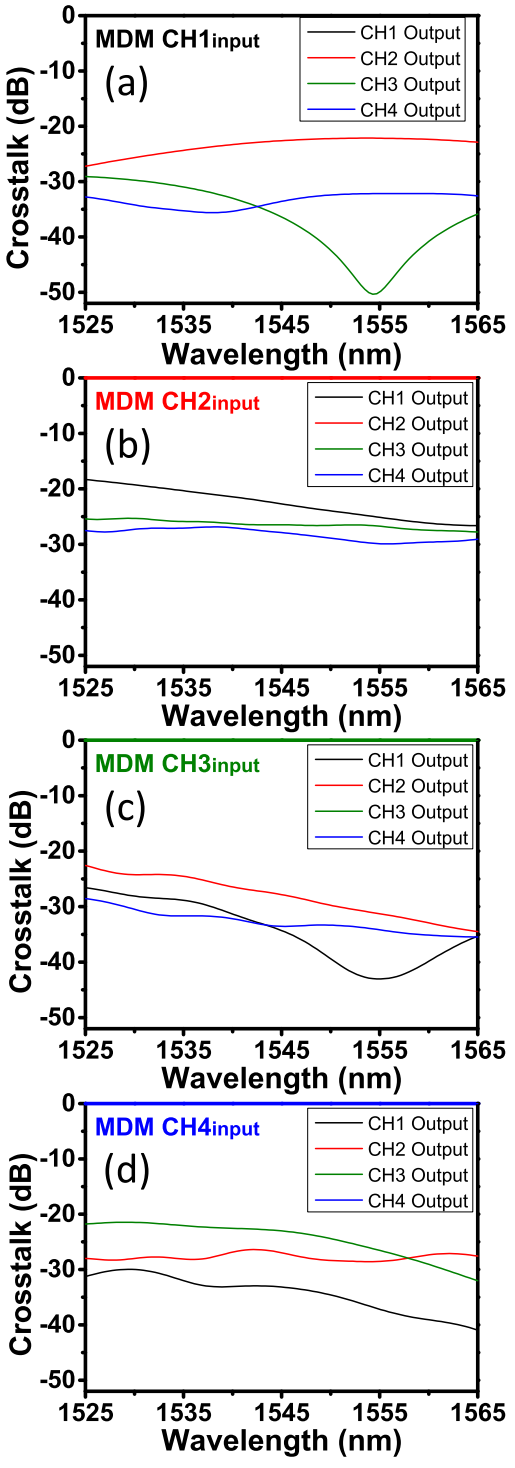


**FIGURE 5.** Simulated mode crosstalk at output ports while the input optical signal is launched at (a) CH1, (b) CH2, (c) CH3 and (d) CH4 in the proposed size reduced MDM MUX/DEMUX device.

MDM-CH1 output. Hence, the optical spectrum at the MDM-CH1 output is flat, while the optical spectra at other output ports show the mode crosstalk.

Figs. 6(a)-(d) show the measured mode crosstalk at different MDM outputs when the optical signal is launched at MDM channel 1 (CH1) to channel 4 (CH4) respectively in the traditional MDM MUX and DEMUX. We can observe that the mode crosstalk are $<-20$ dB in most of the transmission window from 1530 nm to 1565 nm. The highest mode crosstalk is observed when the optical signal is launched at the

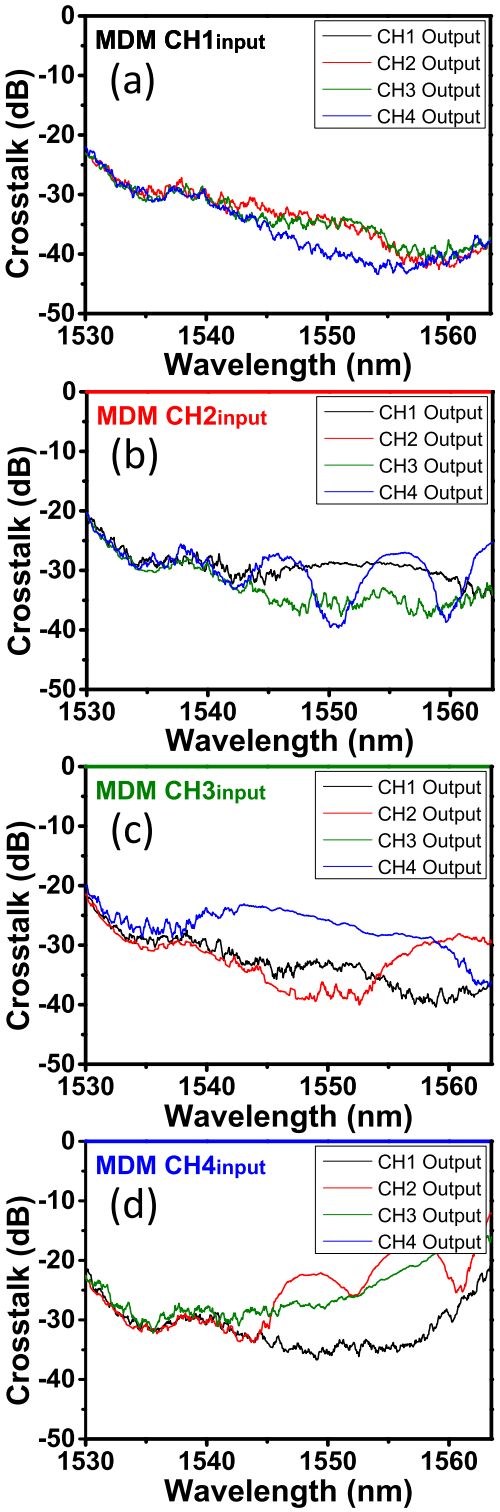


**FIGURE 6.** Measured mode crosstalk at output ports while the input optical signal is launched at (a) CH1, (b) CH2, (c) CH3 and (d) CH4 in the traditional MDM MUX/DEMUX device.

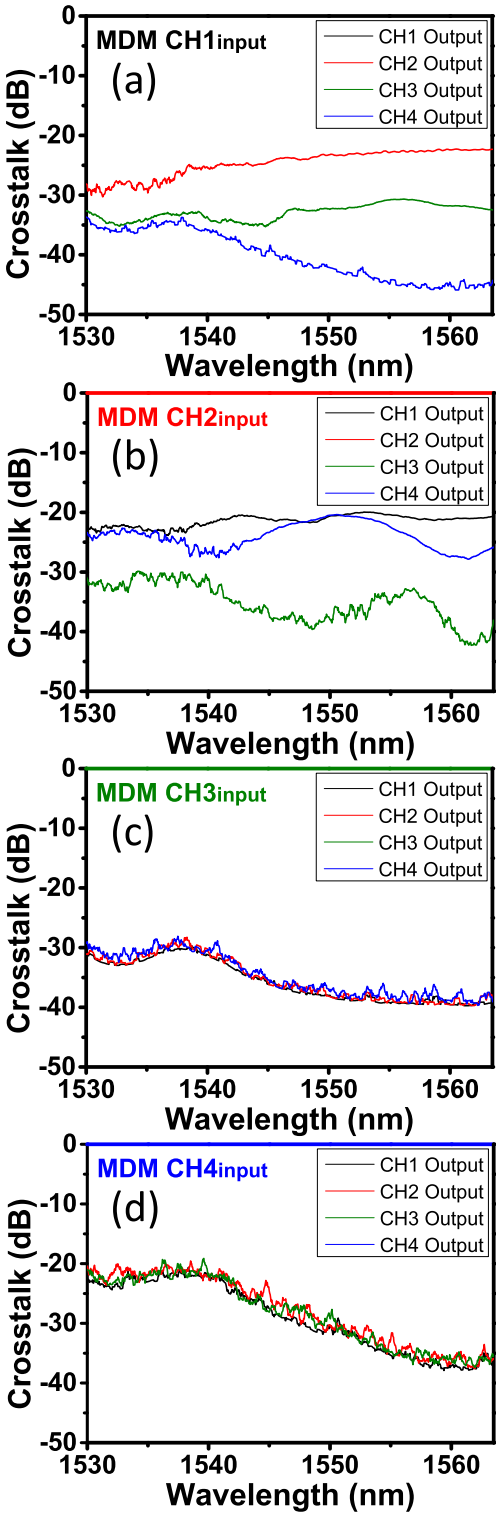


**FIGURE 7.** Measured mode crosstalk at output ports while the input optical signal is launched at (a) CH1, (b) CH2, (c) CH3 and (d) CH4 in the proposed footprint reduced MDM MUX/DEMUX device.

input of MDM CH4 at wavelength >1560 nm. Figs. 7(a)-(d) shows the measured mode crosstalk at different MDM outputs in the proposed footprint reduced MDM MUX and DEMUX. We can also observe that the mode crosstalk are $<-20$ dB in most of the transmission window from 1530 nm to 1565 nm. In previous study [27], the BER performance

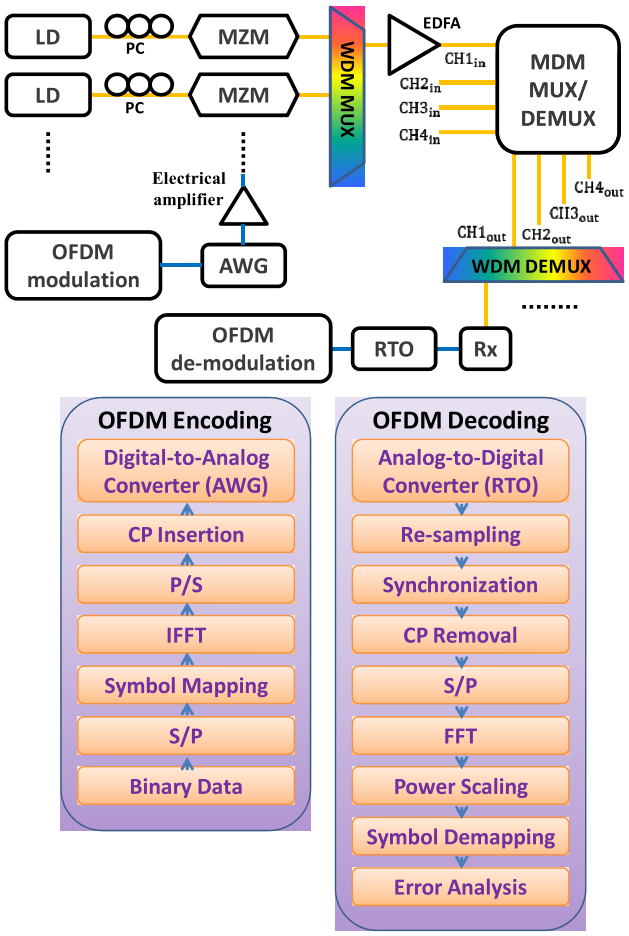


**FIGURE 8.** Architecture of high-speed MDM OFDM signal transmission using the proposed MDM MUX and DEMUX. LD: laser, PC: polarization controller, MZM: Mach-Zehnder modulator, AWG: arbitrary waveform generator, EDFA: erbium-doped fiber amplifier, and RTO: real-time oscilloscope.

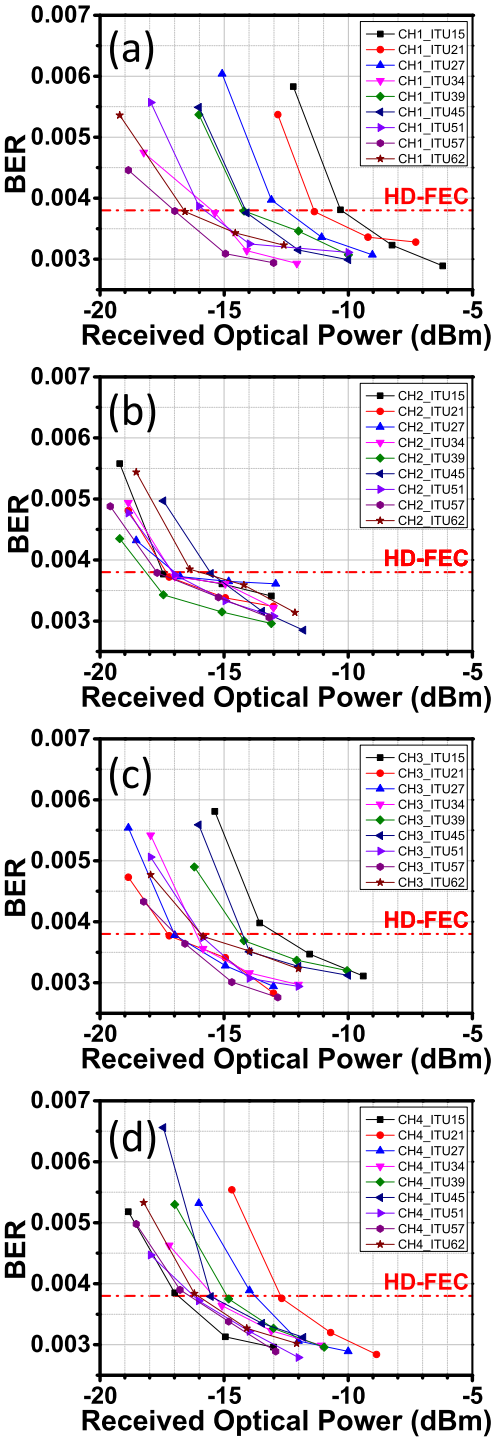


**FIGURE 9.** Measured BER performances of arbitrarily selected wavelength channels of the proposed MDM MUX/DEMUX launching at (a) CH1, (b) CH2, (c) CH3 and (d) CH4.

degradation is negligible if the mode crosstalk is $<-18$ dB. Hence, both MDM devices are good enough for the high-speed and broadband operation. Moreover, we can observe that by reduction of the coupling length by $\sim$80 % in the proposed device, similar mode MUX and DEMUX performance can be observed.

Fig. 8 illustrates the architecture of high-speed MDM OFDM signal transmission using the proposed MDM MUX and DEMUX. The laser (LD) linewidth is $<$100 kHz. The output power of the LD is 6 dBm. An EDFA with noise figure of 4 dB is used to compensate the insertion loss of the MZM and the GCs of the MDM device. The optical input power to the MDM device is 8 dBm. Off-line Matlab®program is used to generate the OFDM signal. The OFDM signal is then encoded onto the optical signal emitted by the LD via a Mach-Zehnder modulator (MZM). For adjacent channels, we can employ different optical delays to de-correlate the channels.

The OFDM signal encoding process includes serial-to-parallel (S/P) conversion of random data, symbol mapping (SM) to different quadrature-amplitude-modulation (QAM) levels, inverse fast Fourier transform (IFFT), parallel-to-serial (P/S) conversion and cyclic prefix (CP) insertion. The generated OFDM signal is then applied to the MZM via a digital-to-analog converter, which is an arbitrary waveform generator (AWG, Tektronix AWG70001A). The AWG has a

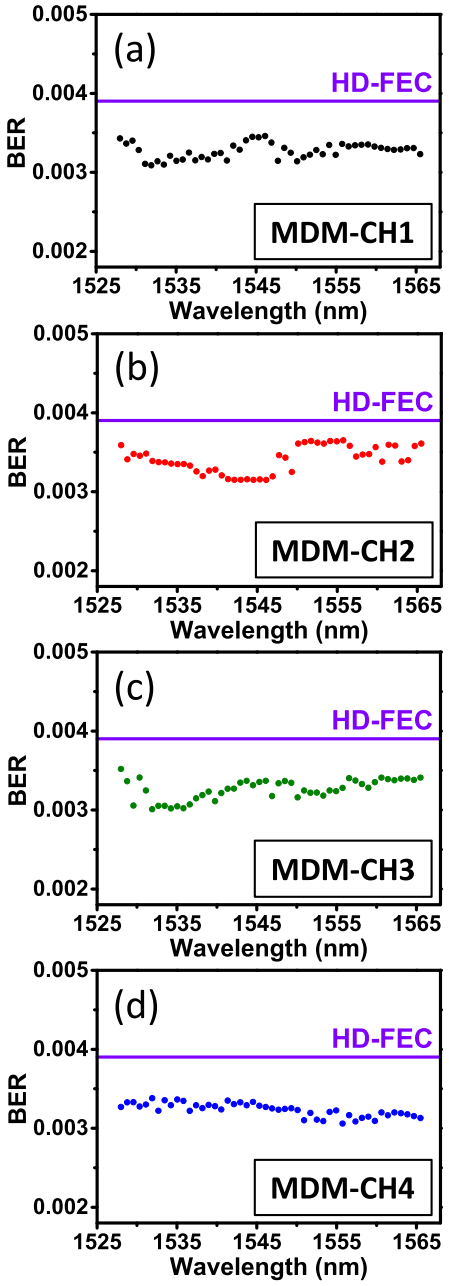


**FIGURE 10.** Measured BER of all the 48 DWDM wavelength channels at MDM output ports of (a) CH1, (b) CH2, (c) CH3 and (d) CH4.

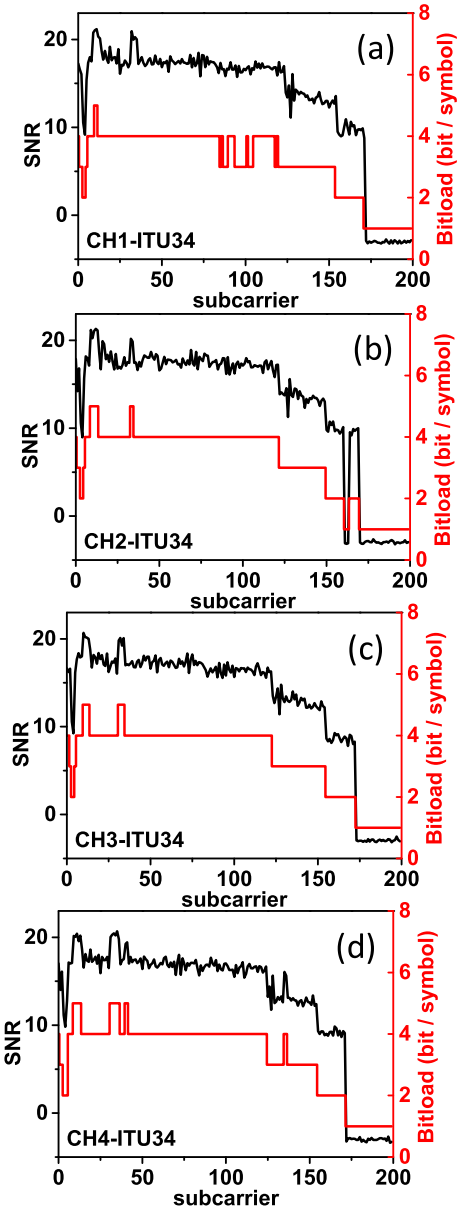


**FIGURE 11.** SNR performances and bit-loading applied to each OFDM subcarrier at wavelengths: 1550.12 nm of the MDM (a) CH1, (b) CH2, (c) CH3 and (d) CH4.

50 GS/s sampling rate, 8 bit resolution and 20 GHz analog bandwidth. The fast-Fourier transform (FFT) size is 512 and the cyclic prefix (CP) is 16. After the mode multiplexing and demultiplexing, the OFDM signal is detected by a photodiode (PD, u2t XPDV2140R) connected to a real-time oscilloscope (RTO, Teledyne LeCroy SDA 816Zi-B). Here, the RTO acts as an analog-to-digital converter converting the analog waveform captured by the PD into digitized signals. The OFDM signal decoding process includes re-sampling, synchronization, CP removal, S/P conversion, FFT, power scaling, symbol de-mapping, and error analysis. The BER is measured using bit-by-bit comparison between the received signal and transmitted signal. The RTO has a 80 GS/s sampling rate and 16 GHz analog bandwidth.

To further enhance the per channel data rates, bit-loading technique based on received signal-to-noise ratio (SNR) of OFDM subcarrier is implemented. 48 wavelength channels from 1527.99 nm to 1565.50 nm are chosen and coupled in and out the MDM MUX and DEMUX via $10^{o}$ off-vertical GCs. Each GC has the coupling loss of $<3$ dB and the optimal center wavelength at 1555 nm.

The measured bit-error ratio (BER) performances of OFDM signals multiplexed and demultiplexed by the proposed devices are illustrated in Figs. 9(a)-(d). We arbitrarily

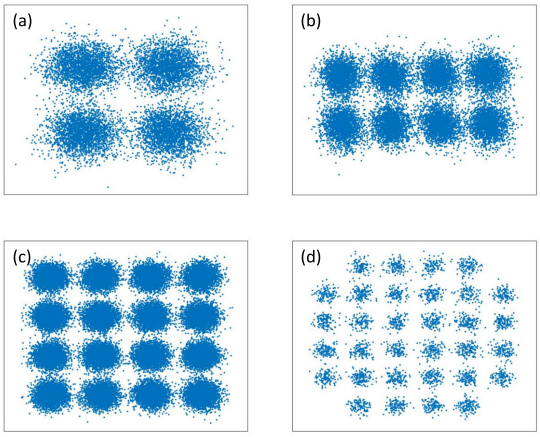


**FIGURE 12.** Measured constellation diagrams of (a) 4-QAM, (b) 8-QAM, (c) 16-QAM and (d) 32-QAM.

select several wavelength channels from different regions in the C-band window: 1527.99 nm(ITU-62), 1531.90 nm(ITU-57), 1536.61 nm(ITU-51), 1541.35 nm(ITU-45), 1546.12 nm (ITU-39), 1550.12 nm(ITU-34), 1555.75 nm(ITU-27), 1560.61 nm(ITU-21) and 1565.50 nm(ITU-15).It is worth to mention that in our BER measurement experiment, our BER evaluation algorithm is to achieve the highest possible OFDM transmission data rate for each channel and at the same time satisfying the FEC threshold. To achieve a higher data rate, bit-loadings to different OFDM subcarriers are applied. However, higher OFDM data rate will decrease the receiver sensitivity. This means that for example in Fig. 9(a), the channel with a lower receiver sensitivity does not necessary mean that it performance is poorer. This is because this channel would carry a higher data rate.

We measure all the 48 wavelength channels, and their BER performances are shown in Figs. 10(a)-(d). The results show that the pre-FEC BER of all the channels (ranging between 1527.99 nm to 1565.50 nm) can satisfy the FEC threshold (BER $3.8 \times 10^{-3}$). The average data rates of MDM CH1 to MDM CH4 for all the 48 DWDM wavelength channels are 60.63 Gbit/s, 59.62 Gbit/s, 62.14 Gbit/s and 62.02 Gbit/s respectively, and a total capacity of 11.73 Tbit/s MDM signal transmission is achieved. The average receiver sensitivities at the FEC threshold of MDM-CH1, MDM-CH2, MDM-CH3 and MDM-CH4 are −13.8 dBm, −16.7 dBm, −15.0 dBm and −14.9 dBm respectively.

Bit-loading algorithm is applied to enhance the data rate. Figs. 11(a)-(d) illustrate one example of the MDM multiplexed and demultiplexed channel (1550.12 nm), showing the SNRs and bit-loaded of the 200 OFDM subcarriers. Half of the OFDM carriers can achieve bit-loading of 4 bit/symbol, representing 16-quadrature amplitude modulation (QAM). The drop of bit-loading level at low frequencies is due to the direct-current (DC) cut-off of the electrical amplifier used. The drop of bit-loading level at high frequencies is due to the limited modulation bandwidths of the electrical devices, such as MZM, electrical amplifier and PD. The data rates of this channel at MDM CH1 to CH4 are 61.84 Gbit/s, 61.93 Gbit/s, 60.51 Gbit/s and 62.41 Gbit/s respectively. Figs. 12(a)-(d) illustrated the measured constellation diagrams of 4-QAM to 32-QAM, corresponding to 2 bit/symbol to 5 bit/symbol.

## IV. CONCLUSION

MDM can increase the total on-chip transmission capacity. SOI based MDM MUX and DEMUX based on ADCs are promising; however, they usually require long coupling lengths for mode conversion. Here, for the first time, we proposed and demonstrated a size reduced SOI based $4 \times 4$ MDM MUX and DEMUX using EEC. By reducing the dimension of the ADC access coupling region, evanescent-wave coupling is enhanced. In the proposed device, the coupling lengths were significantly reduced by 82.2 %, 80.8 % and 76.6 % in CH2, CH3 and CH4 respectively; while the bus waveguide widths are reduced by 20.6 %, 20.1% and 19.1%, respectively. Similar MDM MUX and DEMUX performances were observed in the traditional and the proposed MDM devices, with mode crosstalk $< -20$ dB in most of the C-band window. To illustrate the broadband and high-speed operations of the proposed device, 48 wavelength channels each modulated with $>60$ Gbit/s bit-loaded OFDM signals were successfully mode multiplexed and demultiplexed. A total capacity of 11.73 Tbit/s signal transmission was achieved, satisfying the FEC threshold.

## REFERENCES

[1] G.-K. Chang, A. Chowdhury, Z. Jia, H.-C. Chien, M.-F. Huang, J. Yu, and G. Ellinas, "Key technologies of WDM-PON for future converged optical broadband access networks [Invited]," *J. Opt. Commun. Netw.*, vol. 1, no. 4, p. C35, 2009.

[2] I. C. Lu, C. C. Wei, W. J. Jiang, H. Y. Chen, Y. C. Chi, Y. C. Li, D. Z. Hsu, G. R. Lin, and J. Chen, "20-Gbps WDM-PON transmissions employing weak-resonant-cavity FPLD with OFDM and SC-FDE modulation formats," *Opt. Exp.*, vol. 21, pp. 8622–8629, 2013.

[3] H. H. Lu, H. C. Peng, W. S. Tsai, C. C. Lin, S. J. Tzeng, and Y. Z. Lin, "Bidirectional hybrid CATV/radio-over-fiber WDM transport system," *Opt. Lett.*, vol. 35, pp. 279–281, 2010.

[4] S. Shen, J.-H. Yan, P.-C. Peng, C.-W. Hsu, Q. Zhou, S. Liu, S. Yao, R. Zhang, K.-M. Feng, J. Finkelstein, and G.-K. Chang, "Polarization-Tracking-Free PDM supporting hybrid digital-analog transport for fixed-mobile systems," *IEEE Photon. Technol. Lett.*, vol. 31, no. 1, pp. 54–57, Jan. 1, 2019.

[5] K. Yamada, J. Michel, M. Romagnoli, and H. K. Tsang, "Introduction for the group-IV photonics feature," *Photon. Res.*, vol. 2, no. 3, p. GP1, 2014.

[6] M. Zadka, Y.-C. Chang, A. Mohanty, C. T. Phare, S. P. Roberts, and M. Lipson, "On-chip platform for a phased array with minimal beam divergence and wide field-of-view," *Opt. Exp.*, vol. 26, no. 3, p. 2528, 2018.

[7] T. C. Tzu, Y. Hsu, C. Y. Chuang, X. Wu, C. W. Chow, J. Chen, C. H. Yeh, and H. K. Tsang, "Equalization of PAM-4 signal generated by silicon microring modulator for 64-Gbit/s transmission," *J. Lightw. Technol.*, vol. 35, no. 22, pp. 4943–4948, Nov. 15, 2017.

[8] K. Xu, L.-G. Yang, J.-Y. Sung, Y. M. Chen, Z. Z. Cheng, C.-W. Chow, C.-H. Yeh, and H. Ki Tsang, "Compatibility of silicon mach-zehnder modulators for advanced modulation formats," *J. Lightw. Technol.*, vol. 31, no. 15, pp. 2550–2554, Aug. 2013.

[9] Y. Tong, Q. Zhang, X. Wu, C. W. Chow, C. Shu, and H. K. Tsang, "Integrated germanium-on-silicon Franz-Keldysh vector modulator used with a Kramers-Kronig receiver," *Opt. Lett.*, vol. 43, pp. 4333–4336, 2018.

[10] G.-H. Chen, C.-W. Chow, C.-H. Yeh, C.-W. Peng, P.-C. Guo, J.-F. Tsai, M.-W. Cheng, Y. Tong, and H. K. Tsang, "Mode-Division-Multiplexing (MDM) of 9.4-Tbit/s OFDM signals on Silicon-on-Insulator (SOI) platform," *IEEE Access*, vol. 7, pp. 129104–129111, 2019.

[11] H. Xie, Y. Liu, Y. Wang, Y. Wang, Y. Yao, Q. Song, J. Du, Z. He, and K. Xu, "An ultra-compact 3-dB power splitter for three modes based on pixelated meta-structure," *IEEE Photon. Technol. Lett.*, vol. 32, no. 6, pp. 341–344, Mar. 15, 2020.

[12] S. Han, W. Chen, H. Hu, Z. Cheng, and T. Liu, "Characterization method of a mid-infrared graphene-on-silicon microring with a monochromatic laser," *J. Opt. Soc. Am. B*, vol. 37, pp. 1683–1688, 2020.

[13] X. Chen and H. K. Tsang, "Polarization-independent grating couplers for silicon-on-insulator nanophotonic waveguides," *Opt. Lett.*, vol. 36, pp. 796–798, 2011.

[14] Y. Tong, G. H. Chen, Y. Wang, Z. Zhang, D. W. U. Chan, C. W. Chow, and H. K. Tsang, "1.12-Tbit/s PAM-4 enabled by a silicon photonic transmitter bridged with a 7-Channel MCF," *IEEE Photon. Technol. Lett.*, vol. 32, no. 16, pp. 987–990, Aug. 15, 2020.

[15] W. V. Sorin, B. Y. Kim, and H. J. Shaw, "Highly selective evanescent modal filter for two-mode optical fibers," *Opt. Lett.*, vol. 11, pp. 581–583, Dec. 1986.

[16] D. Ge, Y. Gao, Y. Yang, L. Shen, Z. Li, Z. Chen, Y. He, and J. Li, "A 6-LP-mode ultralow-modal-crosstalk double-ring-core FMF for weakly-coupled MDM transmission," *Opt. Commun.*, vol. 451, pp. 97–103, Nov. 2019.

[17] R. C. Youngquist, J. L. Brooks, and H. J. Shaw, "Two-mode fiber modal coupler," *Opt. Lett.*, vol. 9, no. 5, pp. 177–179, May 1984.

[18] F. Ren, D. Ge, J. Li, Z. Li, Y. He, and Z. Chen, "An all-fiber mode converter assisted by coiled-fiber long-period grating," *Opt. Commun.*, vol. 360, pp. 15–19, Feb. 2016.

[19] S. G. Leon-Saval, T. A. Birks, J. Bland-Hawthorn, and M. Englund, "Single-mode performance in multimode fibre devices," *Proc. OFC*, Anaheim, CA, USA, 2005, p. 25.

[20] N. K. Fontaine, B. Ercan, R. Ryf, J. Bland-Hawthorn, J. R. S. Gil, and S. G. Leon-Saval, "Mode-selective dissimilar fiber photonic-lantern spatial multiplexers for few-mode fiber," in *Proc. 39th Eur. Conf. Exhib. Opt. Commun. (ECOC)*, London, U.K., 2013, pp. 1–3.

[21] S. Randel, R. Ryf, A. Sierra, P. J. Winzer, A. H. Gnauck, C. A. Bolle, R. J. Essiambre, D. W. Peckham, A. McCurdy, and R. Lingle, "6×56-Gb/s mode-division multiplexed transmission over 33-km few-mode fiber enabled by 6×6 MIMO equalization," *Opt. Exp.*, vol. 19, pp. 16697–16707, Dec. 2011.

[22] T. Uematsu, Y. Ishizaka, Y. Kawaguchi, K. Saitoh, and M. Koshiba, "Design of a compact two-mode Multi/Demultiplexer consisting of multimode interference waveguides and a wavelength-insensitive phase shifter for mode-division multiplexing transmission," *J. Lightw. Technol.*, vol. 30, no. 15, pp. 2421–2426, Aug. 2012.

[23] H. D. Tam Linh, T. C. Dung, K. Tanizawa, D. D. Thang, and N. T. Hung, "Arbitrary $TE_0$/$TE_1$/$TE_2$/$TE_3$ mode converter using 1×4 Y-Junction and 4×4 MMI couplers," *IEEE J. Sel. Top. Quan. Electron.*, vol. 26, no. 2, Mar./Apr. 2020, Art. no. 8300708.

[24] S. Bagheri and W. M. J. Green, "Silicon-on-insulator mode-selective add-drop unit for on-chip mode-division multiplexing," in *Proc. 6th IEEE Int. Conf. Group IV Photon.*, Sep. 2009, pp. 166–168.

[25] D. Dai, J. Wang, and Y. Shi, "Silicon mode (de)multiplexer enabling high capacity photonic networks-on-chip with a single-wavelength-carrier light," *Opt. Lett.*, vol. 38, no. 9, pp. 1422–1424, 2013.

[26] J. Wang, S. He, and D. Dai, ""On chip silicon 8 channel hybrid (de) multiplexer enabling simultaneous mode and polarization division multiplexing," *Laser Photon. Rev.*, vol. 8, pp. L18–L22, 2014.

[27] Y. Hsu, C.-Y. Chuang, X. Wu, G.-H. Chen, C.-W. Hsu, Y.-C. Chang, C.-W. Chow, J. Chen, Y.-C. Lai, C.-H. Yeh, and H. K. Tsang, "2.6 Tbit/s on-chip optical interconnect supporting Mode-Division-Multiplexing and PAM-4 signal," *IEEE Photon. Technol. Lett.*, vol. 30, no. 11, pp. 1052–1055, Jun. 1, 2018.

[28] C.-L. Li, X.-H. Jiang, Y. Hsu, G.-H. Chen, C.-W. Chow, and D.-X. Dai, "Ten-channel mode-division-multiplexed silicon photonic integrated circuit with sharp bends," *Frontiers Inf. Technol. Electron. Eng.*, vol. 20, no. 4, pp. 498–506, Apr. 2019.

[29] G. H. Chen, C. W. Peng, M. W. Cheng, P. C. Guo, J. F. Tsai, Y. Tong, C. W. Chow, C. H. Yeh, and H. K. Tsang, "Silicon-photonics based remote-radio-head using mode and wavelength division multiplexing with capacity of 4.781 Tbit/s for radio-over-fiber massive MIMO," *Proc. ECOC*, Dublin, Ireland, 2019, pp. 1–3, doi: 10.1049/cp.2019.0746.


**GUAN-HONG CHEN** received the B.S. degree from the Department of Photonics, National Sun Yat-sen University, Kaohsiung, Taiwan, in 2016. He is currently pursuing the Ph.D. degree with the Department of Photonics, National Chiao Tung University, Hsinchu, Taiwan. His research interests include silicon photonics, optical fiber communications, radio access networks, and advanced modulation formats using for high-speed optical transmission on chip.

**JUI-FENG TSAI** received the B.S. degree from the Department of Optics and Photonics, National Central University, Taiwan, and the master's degree from the Department of Photonics, National Chiao Tung University, Taiwan.

**CHING-WEI PENG** received the B.S. degree from the National Central University, Taiwan. He is currently pursuing the Ph.D. degree with the Department of Photonics, National Chiao Tung University, Taiwan. His research interests include silicon photonics, machine learning for optical communications, and optical coherent communication.

**PIN-CHENG KUO** received the B.S. degree from the Department of Physics, National Central University, Taiwan. He is currently pursuing the Ph.D. degree with the Department of Photonics, National Chiao Tung University, Taiwan. His research interests include silicon photonics and multiplexer design for few-mode fiber (FMF) transmission.

**CHUN-JUI CHEN** received the B.S. degree from the Department of Photonics, National Sun Yat-sen University, Kaohsiung, Taiwan. He is currently pursuing the master's degree with the Department of Photonics, National Chiao Tung University, Taiwan. His research interest includes sub-wavelength structure design for silicon photonics.

**CHI-WAI CHOW** (Senior Member, IEEE) received the B.Eng. degree (Hons.) and the Ph.D. degree from the Department of Electronic Engineering, The Chinese University of Hong Kong (CUHK), in 2001 and 2004, respectively. His Ph.D. degree focused on optical label controlled packet switched networks. After graduation, he was appointed as a Postdoctoral Fellow with the CUHK, working on hybrid integration of photonic components and silicon waveguides. From 2005 to 2007, he was a Postdoctoral Research Scientist, working mainly on two European Union Projects: Photonic Integrated Extended Metro and Access Network (PIEMAN) and Transparent Ring Interconnection Using Multi-wavelength PHotonic switches (TRIUMPH) with the Tyndall National Institute and Department of Physics, University College Cork (UCC), Ireland. In August 2007, he joined the Department of Photonics, National Chiao Tung University, Taiwan, as an Assistant Professor, where he is currently a Professor. He served for many international conferences, including the TPC of OFC 2021, TPC of ECOC 2021, TPC of ECOC 2020, workshop co-organizer of IEEE GLOBECOM 2020, Track Chair of OECC 2020, and TPC of CLEO-PR 2020.

**CHIEN-HUNG YEH** (Member, IEEE) received the Ph.D. degree from the Institute of Electro-Optical Engineering, National Chiao Tung University, Taiwan, in 2004. In 2004, he joined the Information and Communications Research Laboratories (ICL), Industrial Technology Research Institute (ITRI), Taiwan, as a Researcher, where he was promoted to a Principal Researcher for leading the ITRI Industrial-Academic Projects, in 2008. In 2014, he joined as a Faculty Member with the Department of Photonics, Feng Chia University, Taiwan, where he is currently a Professor. His research interests include optical fiber communication, fiber laser and amplifier, optical PON access, MMW communication, fiber sensor, and Li-Fi based technologies.

**YINCHIEH LAI** (Member, IEEE) is currently a Professor with the Department of Photonics, National Chiao Tung University (NCTU), Taiwan. From 1999 to 2001, he was on leave with the Industrial Technology Research Institute (ITRI) and acted as the Team Leader of the Optical Fiber Communication Group, Institute of Opto-electronics, ITRI. His research interests include mode-locked fiber lasers, fiber/optical waveguide components, quantum optics, and silicon photonics. He is an OSA Fellow. He was an Associate Editor of the IEEE PHOTONICS JOURNAL.

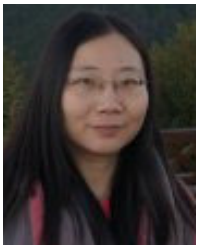

**YANG LIU** received the bachelor's degree from the Department of Electronics Engineering, Northwest University, in 2001, the master's degree from the College of Precision Instrument and Opto-electronics Engineering, Tianjin University, in 2004, and the Ph.D. degree from the Department of Electronic Engineering, The Chinese University of Hong Kong (CUHK), in 2007. Her Ph.D. focused on silicon photonics and nonlinear effects of silicon waveguides. After graduation, she was appointed as a Postdoctoral Fellow with the CUHK. In 2007, she was a Visiting Researcher with the University College Cork, Tyndall National Institute, Ireland. Her research interests include silicon photonics, optical nonlinear effects, visible light communications, and optical wireless communications.